

DOI: 10.1002/cmdc.201200043

Synthesis of Gd and ^{68}Ga Complexes in Conjugation with a Conformationally Optimized RGD Sequence as Potential MRI and PET Tumor-Imaging Probes

Leonardo Manzoni,^{*[a]} Laura Belvisi,^{*[b, c]} Daniela Arosio,^[a] Maria Paola Bartolomeo,^[d] Aldo Bianchi,^[c] Chiara Brioschi,^[d] Federica Buonsanti,^[d] Claudia Cabella,^[d] Cesare Casagrande,^[c] Monica Civera,^[c] Marilena De Matteo,^[c] Lorenza Fugazza,^[e] Luciano Lattuada,^[d] Federico Maisano,^[d] Luigi Miragoli,^[d] Cristina Neira,^[d] Michael Pilkington-Miksa,^[c] and Carlo Scolastico^[b, c]

We report the synthesis of novel chelates of Gd and ^{68}Ga with DPTA, DOTA, HP-DOA3, as well as with AAZTA, a novel chelating agent developed by our research group. These chelating agents were appropriately conjugated, prior to metal complexation, with DB58, an RGD peptidomimetic, conformationally constrained on an azabicycloalkane scaffold and endowed with high affinity for integrin $\alpha_v\beta_3$. Because $\alpha_v\beta_3$ is involved in neo-angiogenesis in solid tumors and is also directly expressed in cancer cells (e.g. glioblastomas, melanomas) and ovarian, breast, and prostate cancers, these constructs could prove

useful as molecular imaging probes in cancer diagnosis by MRI or PET techniques. Molecular modeling, integrin binding assays, and relaxivity assessments allowed the selection of compounds suitable for multiple expression on dendrimeric or nanoparticulate structures. These results also led us to an exploratory investigation of ^{68}Ga complexation for the promising ^{68}Ga -PET technique; the AAZTA complex **15**(^{68}Ga) exhibited uptake in a xenograft model of glioblastoma, suggesting potentially useful developments with new probes with improved affinity.

Introduction

Structural imaging is a powerful tool for detecting the differential features of pathological tissues, particularly of neoplastic formation with respect to the anatomical features of normal tissues. Computed tomography (CT), magnetic resonance imaging (MRI), and ultrasound (US) techniques have thus reached high diagnostic relevance,^[1] especially when reinforced with appropriate contrast agents. The need for early and specific assessment of the manifestation and progression of cancer has prompted the development of functional imaging by techniques that can highlight the metabolic differences of cancer cells. Among these, positron emission tomography (PET) imaging of [^{18}F]2-fluoro-2-deoxy-D-glucose as a marker of high glucose uptake^[2] is the most widely employed. The next conceptual advancement, and now the most promising, has been the targeting of biomolecules that are specifically expressed in tumor cells^[3] such as receptors, adhesion molecules, and enzymes, using high-affinity ligands covalently linked with suitable imaging moieties for radioactive, MRI, or US imaging. This approach has an appealing therapeutic potential, because when proving the specific delivery of imaging moieties to tumor tissues, it opens the way to the design of molecular constructs suitable to concentrate radio- or chemotherapeutic agents in cancer tissues, sparing healthy tissues and organs.

We became particularly interested in targeting $\alpha_v\beta_3$ integrin, a member of the superfamily of integrin adhesion molecules.^[4] This integrin governs the adhesion of endothelial cells to the extracellular matrix (ECM) in the process of angiogenesis under

normal and pathological conditions. In the latter, in tissues claiming increased oxygen and nutrient supplies, such as ischemic and tumor tissues, $\alpha_v\beta_3$ is markedly overexpressed and supports neo-angiogenesis.^[5] In recent years, it has also been observed that $\alpha_v\beta_3$ not only plays a role in cancer progression via angiogenesis, but is also significantly expressed on the

[a] Dr. L. Manzoni, Dr. D. Arosio

Consiglio Nazionale delle Ricerche
Istituto di Scienze e Tecnologie Molecolari
Via Fantoli 16/15, 20138, Milano (Italy)
E-mail: leonardo.manzoni@istm.cnr.it

[b] Dr. L. Belvisi, Prof. C. Scolastico

Università degli Studi di Milano
Dipartimento di Chimica Organica e Industriale
Via Venezian 21, 20133 Milano (Italy)

[c] Dr. L. Belvisi, Dr. A. Bianchi, Prof. C. Casagrande, Dr. M. Civera,

Dr. M. De Matteo, Dr. M. Pilkington-Miksa, Prof. C. Scolastico
Università degli Studi di Milano
Centro Interdipartimentale Studi biomolecolari e applicazioni Industriali
Via Fantoli 16/15, 20138, Milano (Italy)

[d] Dr. M. P. Bartolomeo, Dr. C. Brioschi, Dr. F. Buonsanti, Dr. C. Cabella,

Dr. L. Lattuada, Dr. F. Maisano, L. Miragoli, Dr. C. Neira
Bracco Imaging SpA, Bracco Research Centre
Via Ribes 5, 10010 Colletterto Giacosa (TO) (Italy)

[e] Dr. L. Fugazza

Advanced Accelerator Applications
Via Ribes 5, 10010 Colletterto Giacosa (TO) (Italy)

Supporting information for this article is available on the WWW under <http://dx.doi.org/10.1002/cmdc.201200043>.

outer membranes of certain cancer cells such as glioblastomas, melanomas, and ovarian, breast, and prostate cancers, and is involved in metastasis and proliferation.^[6] Being correlated with disease progression, the expression of $\alpha_v\beta_3$ integrin plays a role as a marker of angiogenesis, tumor development, and metastasis. Therefore, noninvasive visualization of this integrin may provide new means for tumor detection and staging.^[7]

Because $\alpha_v\beta_3$ integrin interacts with ECM and cellular proteins by recognizing and binding at an Arg-Gly-Asp (RGD) sequence,^[8] many research groups have devoted efforts to the development of integrin ligands structurally based on linear and cyclic peptides containing the RGD sequence.^[9] We focused on inserting the RGD motif into rigid peptidomimetic azabicycloalkane scaffolds with varying structural and stereochemical features suitable for imposing specific conformations onto the RGD sequence, in order to select the optimal spatial disposition of the RGD pharmacophoric groups for interaction with the integrin, while minimizing the peptidic features prone to metabolic degradation in vivo.^[10] Accordingly, we synthesized small libraries of cyclic pentapeptide mimics, and in one of these we identified the high-affinity and specific $\alpha_v\beta_3/\alpha_v\beta_5$ integrin ligand ST1646 (Figure 1). Biochemical and pharmacological studies revealed ST1646 as a potent and selective antagonist endowed with significant in vitro and in vivo anti-angiogenic activity,^[10b] suggesting the possibility of therapeutic development of ST1646 for cancer applications.

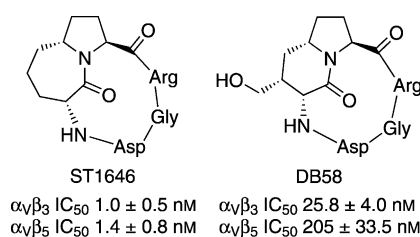


Figure 1. Peptidomimetic integrin ligands ST1646 and DB58 and their IC₅₀ values in the inhibition of biotinylated vitronectin binding to purified receptors.

On the basis of these results, we progressed to new synthetic developments aimed at making azabicycloalkane scaffolds suitable for conjugation with therapeutic or diagnostic molecular moieties. We recently reported a convenient synthesis of conformationally constrained homoSer-Pro dipeptide mimics and their use in the preparation of cyclic RGD compounds.^[11] These cyclic RGD pentapeptide mimics have an etheroalkyl side chain terminated by a hydroxy group that can be easily transformed into various reactive functionalities (amino, azido, thio, etc.), enabling us to conjugate diverse functional units for application in medical diagnosis and therapy.

Among the new compounds, we selected DB58 (Figure 1), which showed the highest affinity for $\alpha_v\beta_3$ integrin in an in vitro binding assay,^[11b] and we conjugated this active ligand to probes for optical imaging (i.e., fluorescein and the near-infrared (NIR) probe Cy5.5).^[12] These conjugates provided us with interesting indications of specific binding on various $\alpha_v\beta_3$ -ex-

pressing cell lines, and, in the case of the NIR probe, of in vivo tumor uptake and persistence in mice xeno-implanted with human glioblastoma U-87 MG cells expressing the integrin. We therefore considered DB58 as an optimal starting point in the development of novel $\alpha_v\beta_3$ -targeted probes in clinically applicable imaging techniques; herein we report the conjugation and complexation of the amino derivative of DB58 with several Gd^{III} chelating moieties for MRI imaging, along with extension to the synthesis of ⁶⁸Ga complexes for PET imaging. Moreover, with the aim of improving the signal-to-noise ratio, a divalent compound featuring two gadolinium complex moieties was synthesized.

MRI contrast agents based on gadolinium complexes are currently employed as diagnostic agents in medicinal imaging.^[13] We therefore decided to exploit the most efficient and clinically validated ligands for gadolinium coordination, based on polyamino polycarboxylic structures such as DOTA, HP-DO3A, and DTPA (Figure 2), which guarantee high thermody-

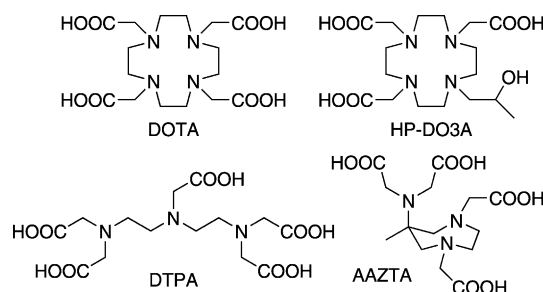


Figure 2. Ligands for gadolinium coordination.

namic and kinetic stability: very important properties for clinical safety.^[14] Gadolinium complexes of DOTA (Dotarem, Guerbet), HP-DO3A (Prohance, Bracco Imaging) and DTPA (Magnevist, Bayer Schering Pharma AG) are examples of stable, extracellular, nonspecific MRI contrast agents with wide clinical application.^[15] We also used AAZTA (Figure 2), a recently reported ligand^[16] that can form a stable gadolinium complex with high relaxivity.

Specificity of targeting of gadolinium complexes can be achieved by conjugating bifunctional derivatives of the chelating agents (see examples in Figure 3) to a moiety, such as a peptide, that is suitable for inducing delivery and accumulation of the MRI probes into specific normal or pathological tissues;^[17] for this study an integrin ligand was used.

Results and Discussion

Chemistry

We first investigated the influence of the distance between the Gd cage and the cyclic RGD ligand on the affinity of the conjugated compounds toward $\alpha_v\beta_3$ integrin. Next, we examined the influence of various chelating agents toward the ability of the Gd complex to lower T₁ values. Finally, we explored the

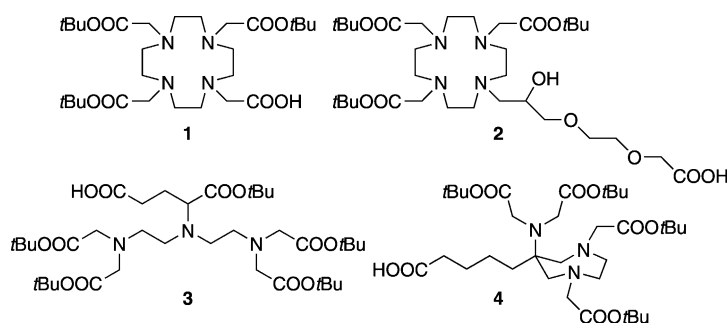


Figure 3. Bifunctional chelating agents.

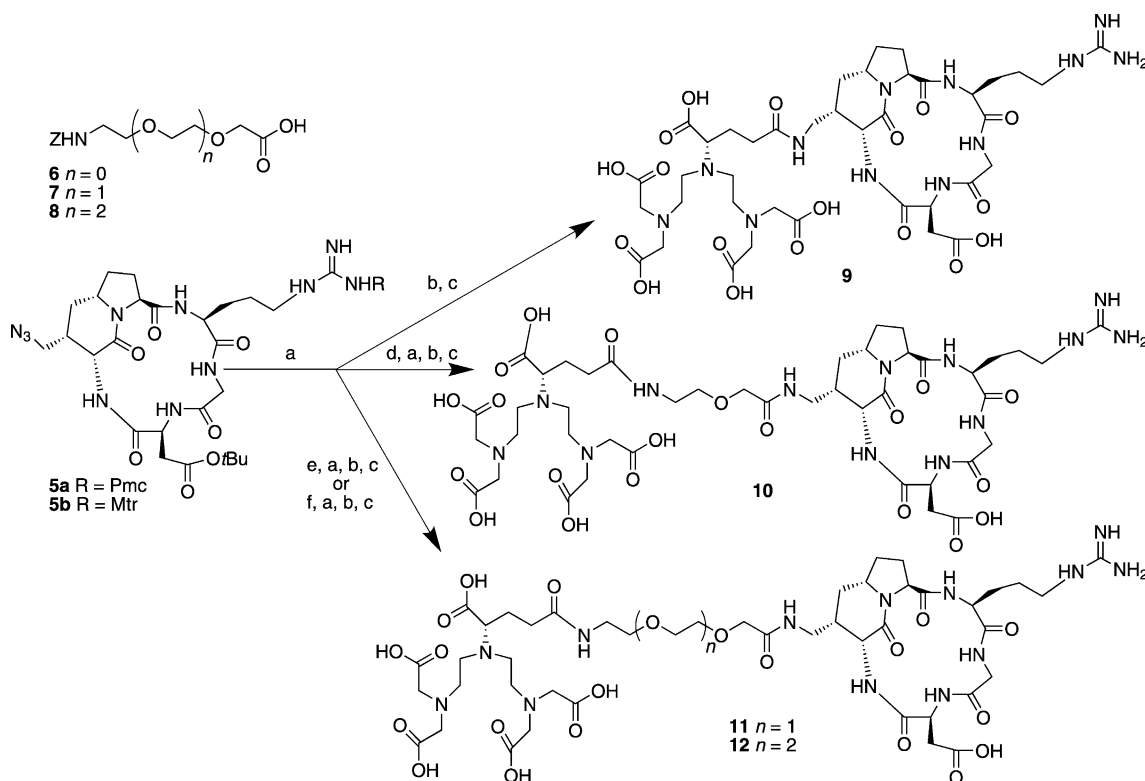
possibility of increasing the signal-to-noise ratio through a divalent presentation of the Gd cage.

For the first aspect, we selected DTPA as the lanthanide chelator and prepared four compounds differing in the distance between the chelating and targeting groups. In compound **9** the chelating cage is conjugated directly to the targeting RGD moiety, whereas in compounds **10–12** three linkers, constituted by varying numbers of ethylene glycol units, are introduced. The synthetic path proceeds from the bifunctional chelating agent **3**, where on a total of six carboxylic groups, five are protected with *tert*-butyl ester, and one is free.^[18] To synthesize compound **9**, the known azide **5a**, derived from DB58,^[11b] was hydrogenated with palladium on carbon, and the corresponding amine was coupled to **3** with standard procedures for amide formation (HBTU, HOBT, DIPEA, DMF)

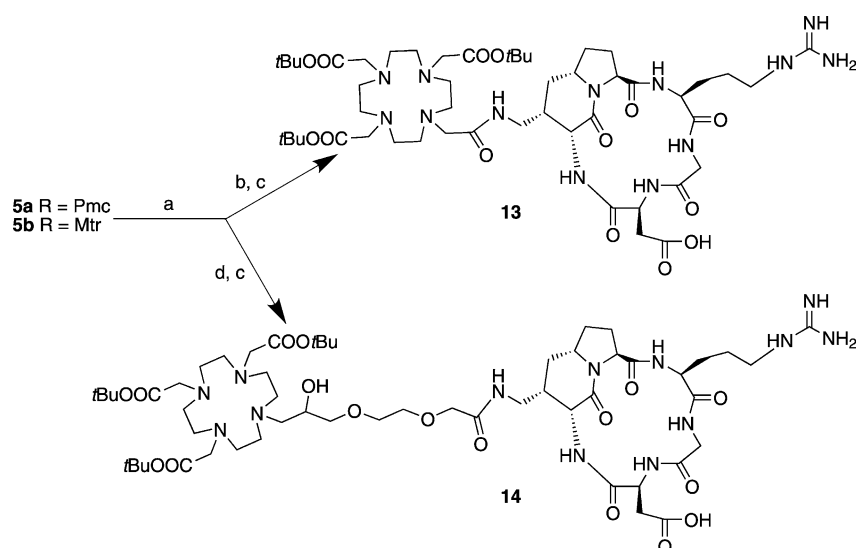
(Scheme 1). In the case of compounds **10–12**, after reduction of the azide, the orthogonally protected spacers **6–8** were conjugated, respectively, and, after nitrogen protecting group removal, coupled with **3** to afford the desired protected compounds. Finally, the side chain protecting groups of the RGD sequence and the five *tert*-butyl esters of the DTPA chelator were removed by standard methods used in peptide chemistry (TIPS, 1,2-ethanedithiol, water, thioanisole, TFA) to furnish the desired compounds **9–12** (52–85% overall yields).

The second aspect we evaluated is the influence of the type of chelating agent on the ability of the Gd^{III} complex to lower the T₁ values. Therefore, we considered a DOTA derivative,^[19] a HP-DO3A derivative,^[20] and an AAZTA derivative (the synthesis of the bifunctional chelating agent **4** is described in the Supporting Information) as gadolinium chelators, and we conjugated them to the RGD mimic. The synthetic route for their preparation is identical to that reported for DTPA derivatives (Scheme 2 and Scheme 3). All final conjugated compounds **9–16** were purified by semi-preparative RP HPLC followed by lyophilization before the complexation with gadolinium.

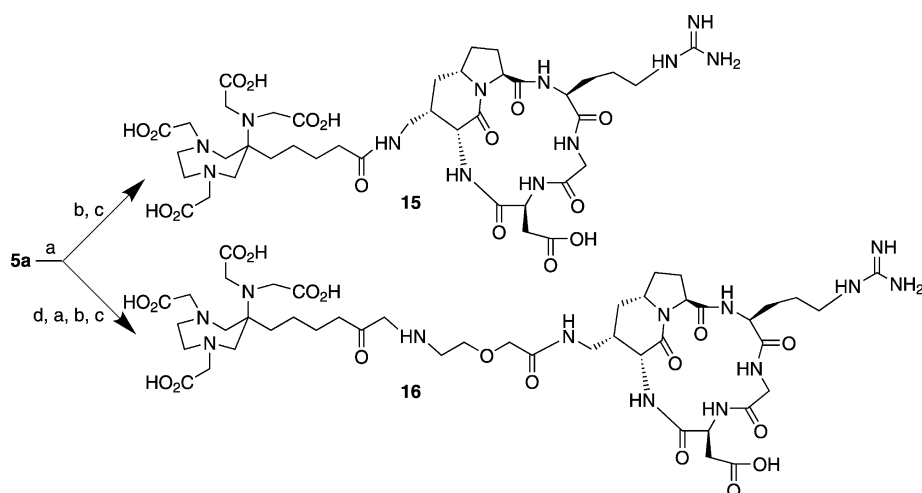
As anticipated, with the aim of improving the signal-to-noise ratio in MRI analysis, we designed a divalent compound featuring two Gd complex moieties. Our approach to the synthesis of divalent systems is based on glutamic acid dendrimers. Compound **17** was easily prepared using glutamic acid as the



Scheme 1. a) H₂, 10% Pd/C, EtOH, RT, 24 h; b) **3**, HOBT, HBTU, DIPEA, DMF, RT, 4–8 h, 58–99% over two steps; c) TIPS/1,2-ethanedithiol/H₂O/thioanisole (2.5:2.5:2.5:5), TFA, RT, 5–6 h, 80–85%; d) **6**, HOAT, HATU, DIPEA, DMF, RT, 24 h, 72%; e) **7**, HOAT, HATU, DIPEA, DMF, RT, 24 h, 95%; f) **8**, HOAT, HATU, DIPEA, DMF, RT, 24 h, 99%.



Scheme 2. a) H_2 , 10% Pd/C, EtOH, RT, 24 h; b) **1**, HOBT, HBTU, DIPEA, DMF, RT, 18 h, 75%; c) TIPS/1,2-ethanedithiol/ H_2O /thioanisole (2.5:2.5:2.5:5), TFA, RT, 5–7 h, 68–70%; d) **2**, HOAT, HATU, DIPEA, DMF, RT, 24 h, 99%.



Scheme 3. a) H_2 , 10% Pd/C, EtOH, RT, 24 h; b) **4**, HOBT, HBTU, DIPEA, DMF, RT, 6–24 h, 99%; c) TIPS/1,2-ethandi-

branching unit, and multiple copies of the chelating agent were bound to this inert branching core (Figure 4).

Commercially available L-Boc glutamic acid was activated with *N*-hydroxysuccinimide (NHS) in the presence of *N,N*-diisopropylcarbodiimide (DIC). The activated ester was coupled with propargylamine to give compound **18**. Removal of the Boc group with trifluoroacetic acid yielded the deprotected amine **19**, ready for the coupling reaction. The azido group of **5b** was hydrogenated with 10% Pd/C to give the corresponding amine, which was treated with succinic anhydride in the presence of DIPEA to give the acid **20**. Activation of the carboxylic group with TBTU and HOBT, followed by coupling with the previously synthesized amine **19** gave the alkynyl derivative **21** (Scheme 4).

Functionalization of the dendrimer ends with DTPA derivative is based on the 1,3-dipolar cycloaddition between terminal triple bonds and azides. The copper(I)-catalyzed reaction is very rapid and completely regioselective. The catalyst is prepared by in situ reduction of $\text{Cu}(\text{OAc})_2$ by sodium L-ascorbate. Thus, azide **22**, which was obtained by coupling compound **3** with the commercially available azido-PEG-amine,

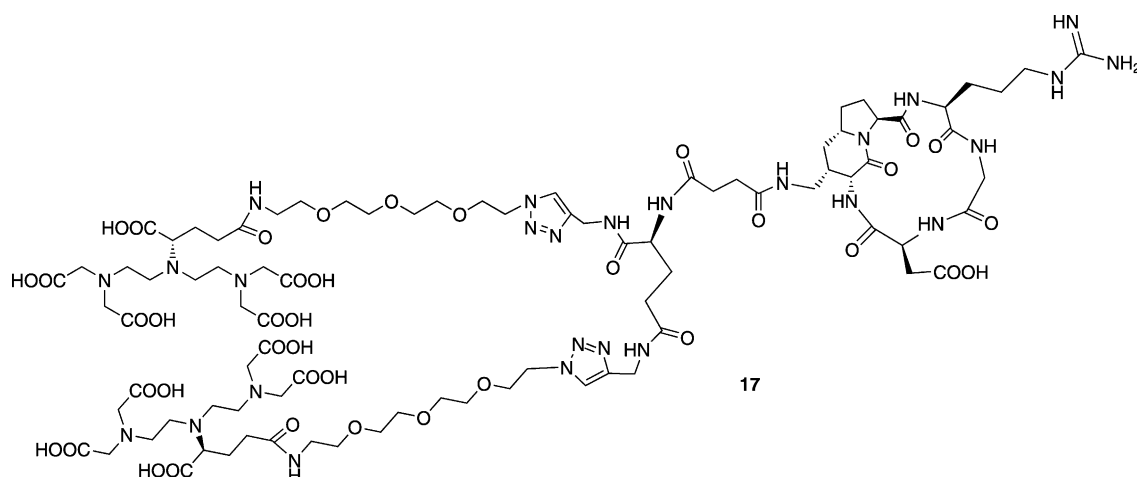
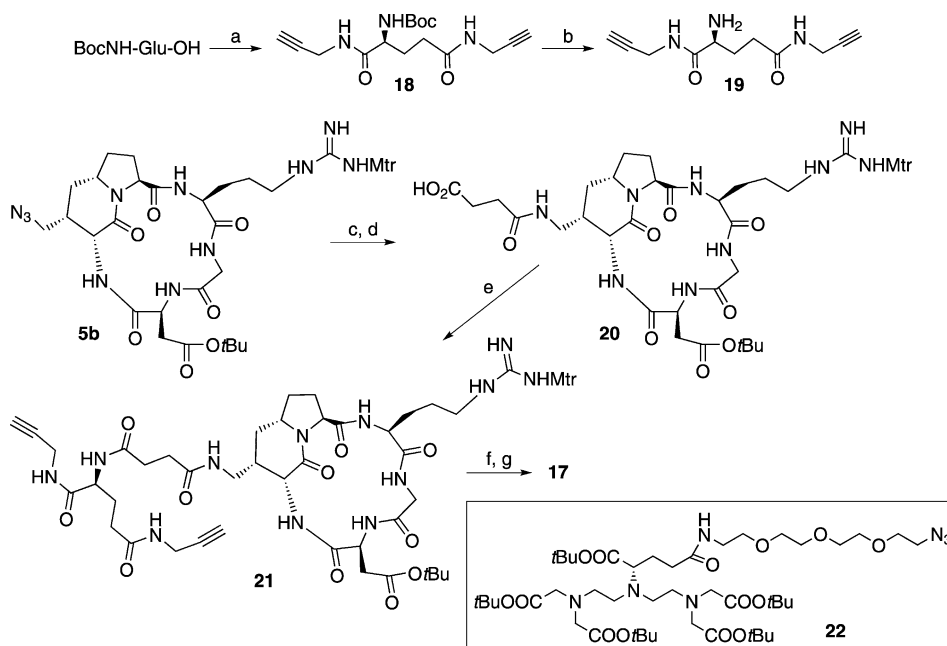


Figure 4. Divalent compound **17** featuring two gadolinium complex moieties.



Scheme 4. a) NHS, DIC, propargylamine, RT, 15 h; b) TFA, CH₂Cl₂, RT, 2 h; c) H₂, 10% Pd/C, MeOH, RT, 24 h, 94%; d) succinic anhydride, DIPEA, THF, RT, 18 h 88%; e) 19, HOBT, TBTU, DIPEA, DMF, RT, 3 h, 77%; f) 22, Cu(OAc)₂, sodium L-ascorbate, *tert*-butanol/H₂O, RT, 42%; g) phenol/thioanisole/1,2-ethanedithiol/H₂O, (5:5:2.5:5), TFA, RT.

was subjected to the cycloaddition reaction conditions in the presence of the protected alkynyl derivative **21** to give divalent protected DTPA dendrimer. Finally, deprotection using a mixture of trifluoroacetic acid, phenol, thioanisole, 1,2-ethanedithiol, and water gave compound **17** (Scheme 4). Complexation of **9–17** with gadolinium afforded Gd-chelated compounds **9(Gd)–17(Gd)** (see Supporting Information).

Synthesis of ⁶⁸Ga-labeled compounds

Labeling of DTPA and AAZTA derivatives **10** and **15**, respectively, with ⁶⁸Ga was performed at pH 3.8; the pH was then corrected to the physiological value, and the final radiochemical purity was assessed. Evaluation of the stability at physiological pH (7.4) of the ⁶⁸Ga complexes **10**(⁶⁸Ga) and **15**(⁶⁸Ga) was performed by HPLC analysis with radiometric detection. Compound **15**(⁶⁸Ga) with the AAZTA coordination cage was observed to be stable under physiological conditions, as the peak of the complex remains clearly detectable (figure S1, Supporting Information) while no free ⁶⁸Ga is observed. For compound **10**(⁶⁸Ga), which differs from **15**(⁶⁸Ga) only in the gallium coordination cage (DTPA instead of AAZTA), HPLC analysis showed that the complex is completely dissociated at pH 7.4 and only the peak of free gallium is present in the chromatogram (figure S2, Supporting Information). Therefore, the complex with the AAZTA coordination cage was chosen for *in vivo* experiments.

Molecular modeling

Monte Carlo conformational searches^[21] (AMBER* force field,^[22] implicit water GB/SA solvation model)^[23] were performed on ligands **9(Gd)** and **10(Gd)** within the X-ray crystal structure of the integrin $\alpha_v\beta_3$ binding site^[24] to evaluate, at the molecular level, the effect of the Gd-chelant unit spacer on the binding of the RGD moiety.

Considering the X-ray structure of cilengitide bound to the $\alpha_v\beta_3$ headpiece (PDB ID: 1L5G) as representative of the optimal RGD interaction mode, conformers of **9(Gd)** and **10(Gd)** were evaluated for their ability to reproduce the experimental binding mode. In the X-ray structure, the acidic and basic moieties of the RGD sequence point in opposite directions, acting like an electrostatic clamp and attaching

to charged regions of the integrin binding site. The positively charged guanidinium group of the Arg residue interacts with the negatively charged side chains of Asp218 and Asp150 in the α unit. One carboxylate oxygen atom of the ligand Asp side chain is coordinated to MIDAS metal cation region of the β unit, while the second carboxylate oxygen atom forms hydrogen bonds with the backbone amides of Asn215 and Tyr122 in the β unit. A hydrogen bond between the ligand Asp NH group and the C=O function of β_3 -Arg216 provides further stabilization to the complex.

Conformers found within 3 kcal mol⁻¹ of the global minimum of ligand **9(Gd)** are positioned within the integrin binding site according to two binding modes. The lowest-energy conformer represents 45% of the Boltzmann-weighted conformer population and displays the Gd cage and the RGD motif both interacting with the β subunit. Relative to the cilengitide RGD interaction mode, the Arg guanidinium group loses the electrostatic interaction with Asp218 and Asp150 side chains of the α subunit. The remaining 55% of conformers form all the key RGD crystallographic interactions with the charged Gd cage directed toward the ADMIDAS region of the β subunit.

In contrast, all the structures found within 3 kcal mol⁻¹ of the global minimum of compound **10(Gd)** form the RGD reference system interactions (Figure 5). The chelant unit is directed toward the outside of the integrin binding site, growing unhindered. In agreement with binding data (Table 1), ligand **10(Gd)** appears to have the optimal linker length to properly fit the RGD sequence and the Gd cage within the $\alpha_v\beta_3$ binding site.

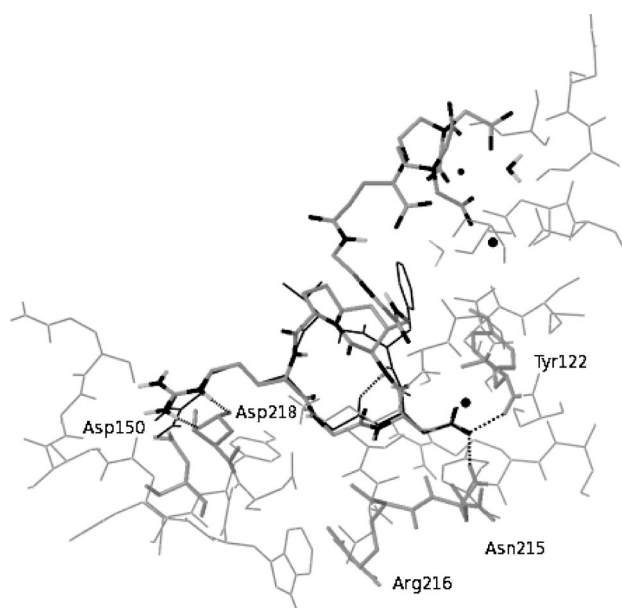


Figure 5. Global minimum of the complex 10(Gd): $\alpha_v\beta_3$ headpiece forming the X-ray interactions. Cilengitide is in black wire and 10(Gd) is in tube representation (O, N, Gd in black; C in gray and polar hydrogen atoms in light gray). Receptor is in gray wire representation, with interacting key residues highlighted as tubes and metal ions shown as black spheres. Nonpolar hydrogen atoms are removed for clarity.

Table 1. IC_{50} values of Gd-chelated RGD derivatives.

Compound	IC_{50} [nM] ^[a]
DB58	26 ± 4
9(Gd)	270 ± 140
10(Gd)	30 ± 11
11(Gd)	54 ± 24
12(Gd)	130 ± 64
13(Gd)	> 1000
14(Gd)	830 ± 120
15(Gd)	290 ± 65
16(Gd)	570 ± 110
17(Gd)	450 ± 22

[a] Values represent the mean ± SE from 2–3 replicate assays carried out in triplicate.

Binding affinity evaluation

All synthesized products were evaluated after complexation with Gd^{III}. Affinity for the receptor was measured by the ability to compete with vitronectin, a natural target in the extracellular matrix, for the binding to immobilized purified human $\alpha_v\beta_3$ integrin.^[9a] Accordingly, we calculated the IC_{50} values, which represent the peptide concentrations required to inhibit 50% of vitronectin binding to the receptor.

The peptides were able to partially or completely suppress binding of the natural ligand to the isolated receptor, and the binding curves followed the expected sigmoidal pattern. Comparing the IC_{50} data (Table 1) with structural features of the linear chelating compounds, it is apparent that the presence of a linker that is too short (9(Gd)) or too long (12(Gd)) decreases

binding affinity. The presence of a mid-length linker (in 10(Gd) and 11(Gd)) maintains affinity at the same level of the unconjugated compound (DB58), possibly because it keeps the ligand cage distal from the RGD binding site. At the other extreme, a spacer that is too long, as in 12(Gd), may also be detrimental to binding because the high spacer flexibility allows interference of the Gd complex with the RGD side of the molecule.

Rather unexpectedly, the presence of a cyclic ligand, i.e., DOTA, HP-DO3A, or AAZTA, markedly decreased binding affinity, resulting in IC_{50} values consistently > 100 nM. Moreover, further increases to the bulkiness of the derivatives deteriorated binding properties, as can be observed by comparing the mono-DTPA derivatives with 17(Gd), which carries two Gd-DTPA units.

Relaxivity data

The Gd-chelated RGD derivatives were characterized by relaxometry. Table 2 shows the millimolar relaxivity at 20 MHz, 25 °C for each tested compound. Fittings of the NMRD profiles (fig-

Table 2. Relaxometric characterization of Gd-chelated RGD derivatives.

Compound	r_{1p} [mM ⁻¹ s ⁻¹] ^[a]
Gd-DTPA	4.45 ± 0.18
9(Gd)	7.55 ± 0.12
10(Gd)	7.63 ± 0.12
11(Gd)	7.49 ± 0.10
12(Gd)	7.91 ± 0.09
14(Gd)	6.20 ± 0.04
15(Gd)	12.94 ± 0.48
16(Gd)	13.32 ± 0.16
17(Gd)	8.37 ± 0.29

[a] Measurements were acquired at 20 MHz, 25 °C; values represent the mean ± SD from three experiments.

ure S3, Supporting Information) and comparison with the relaxivity behavior as a function of temperature (figure S4, Supporting Information) demonstrated that with respect to Gd-DTPA, the increase in relaxivity observed at all examined fields is a consequence of the increase in molecular reorientation time due to conjugation with the peptide.

As expected from their molecular weights, the r_{1p} values of the Gd-chelated RGD compounds measured at 20 MHz and 25 °C were higher than that of the precursor Gd-DTPA (r_{1p} = 4.45 mM⁻¹s⁻¹). However, the r_{1p} values for the $\alpha_v\beta_3$ integrin ligands were slightly lower than what was expected from the extrapolation of the linear correlation law occurring between r_{1p} and molecular weight for lower-molecular-weight compounds (figure S5, Supporting Information). This is probably due to the presence of intramolecular motions of the peptide moiety that make the molecular reorientation time shorter than what would be expected simply on the basis of molecular weight. For the two Gd-AAZTA conjugates, the relaxivity is higher, as expected for these complexes, which coordinate two water molecules.

PET

In recent studies we achieved good evidence for the value of our RGD-carrying scaffolds *in vivo* by NIR imaging of the Cy5.5-coupled amine derived from compound **5a**,^[12b] showing specific uptake and persistence in the tumor tissue of mice bearing U-87 MG glioblastoma. Glioblastoma, the most frequent subtype of human primary brain tumors, is the target of a phase III trial of cilengitide, the only RGD-based agent in advanced clinical investigations.^[5b] Therefore, we decided to seek, in the same experimental tumor, a proof-of-concept for the present metal-chelated conjugates using ^{68}Ga -PET, which is orders of magnitude more sensitive than Gd-MRI. In our preliminary experiment, the ^{68}Ga -AAZTA RGD conjugate **15**(^{68}Ga) was intravenously injected in mice ($n=3$) and compared with ^{68}Ga -AAZTA ($n=2$). Figure 6 shows representative images of **15**(^{68}Ga) (panel a) and ^{68}Ga -AAZTA (panel b) uptake over time. At each

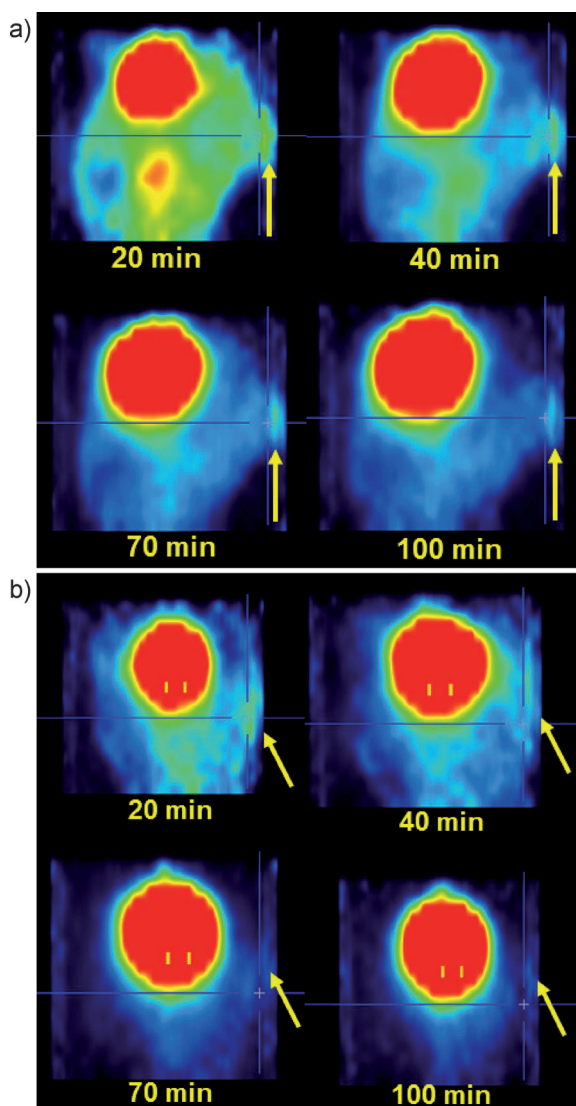


Figure 6. Representative U-87 MG tumor mass images at various time points after administration of a) **15**(^{68}Ga) and b) ^{68}Ga (AAZTA); arrows show the tumor position.

time the coronal section is indicated with a yellow arrow showing the tumor mass. The clearance behavior of the two radiotracers is quite different, with the untargeted molecule being eliminated from the bloodstream more quickly than the targeted one, with a rapid accumulation in the bladder. The ^{68}Ga -AAZTA signal in the tumor is detectable 20 min after administration; it then decreases rapidly, being undetectable ~ 50 min later. On the other hand, **15**(^{68}Ga) has slower kinetics and accumulates in the tumor. In fact, ~ 40 min following injection, the tumor is highlighted and readily detectable due to improved contrast between the tumor mass and the surrounding tissues. The signal remains appreciable in the tumor until 70 min post-injection.

Figure 7 shows the time course of tumor uptake of the two compounds. The RGD conjugate appears to concentrate in tumor tissue and to persist at higher concentrations than the non-targeted molecule up to 150 min. Moreover, by simultaneous injection of the integrin ligand ϵ (RGDfV), the expected competitive antagonism in integrin binding was observed as a decreased uptake of **15**(^{68}Ga), similar to that of the nonspecific compound (Figure 7).

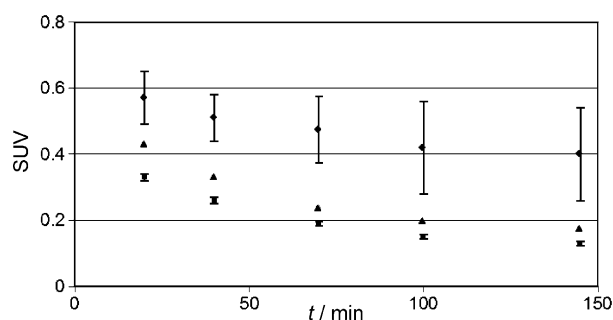


Figure 7. Time course uptake of **15**(^{68}Ga) alone (◆), in co-administration with ϵ (RGDfV) (▲), and ^{68}Ga (AAZTA) (■) in U-87 MG xenograft mice.

Conclusions

Our exploration of chemical diversity in Gd chelates with a constrained RGD ligand showed, in the case of DPTA derivatives, a modulation of the affinity for integrin $\alpha_v\beta_3$ by changes in length of the spacer setting the distance between the chelated Gd ion and the RGD moiety, with good affinity at intermediate length, preserved at the level of the parent ligand DB58 in compound **10**(Gd). The extension of the exploration to DOTA, HP-DO3A, or AAZTA with various linkers, and also with a geminal presentation of two Gd chelates, did not produce compounds with adequate affinity.

Relaxivity, another relevant property of the chelated compounds, definitely increased with respect to DPTA-Gd chelate for all compounds, although less than proportionally with molecular weight, at variance from the correlation reported for a set of non-targeted Gd chelates. It is conceivable that the conformational freedom added by the linker–ligand moiety may allow molecular motions that oppose the increase in relaxivity.

Comparative modeling of compounds **9**(Gd) and **10**(Gd) showed that the fitting of the latter in the integrin $\alpha_v\beta_3$ binding site is in good agreement with the interactions observed in the crystallographic study of cilengitide, whereas the fitting of **9**(Gd) does not completely reproduce the X-ray structure binding mode. The degree of integrin affinity of compound **10**(Gd) is similar to, or somewhat better than, that of the fluorescein-linked analogues we previously reported.^[12a] These had shown selective uptake and internalization in $\alpha_v\beta_3$ -expressing cells.

The current trend for novel targeted Gd contrast agents is toward multiple presentation of Gd atoms, aiming at increased sensitivity of the MRI method.^[25] Thus, we are considering the transfer of the structural features and the Gd–RGD distance of compound **10**(Gd) in multiple moieties bound on dendrimeric or nanoparticulate structures.

Our efforts to transfer the favorable binding properties of **10**(Gd) directly to the complex **10**(⁶⁸Ga), as a tool for PET with ⁶⁸Ga probes (a promising new sensitive and easily accessible PET technique), resulted in a complex unstable under physiological conditions. In contrast, the complexation of ⁶⁸Ga in compound **15**, resulting in the stable complex **15**(⁶⁸Ga), afforded the first targeted AAZTA derivative suitable for in vivo experiments. Notwithstanding the modest binding affinity of the corresponding **15**(Gd) compound, we decided to run a preliminary in vivo experiment in a murine model of human glioblastoma, expressing $\alpha_v\beta_3$, on which we recently reported interesting observations with our Cy5.5-linked DB58-derived NIR probe. The present preliminary observations, within their experimental limitations, are in accordance with the NIR results and indicate a better uptake and persistence in the tumor with respect to the non-targeted AAZTA(⁶⁸Ga) complex. Specificity of targeting was pointed out by the antagonism produced by administration of the $\alpha_v\beta_3$ integrin ligand c(RGDfV). The results suggest additional chemical and biological investigations for improved high-affinity ligands, aiming at the development of clinically applicable integrin-targeted ⁶⁸Ga-PET probes.

Experimental Section

Chemistry

The synthesis of the bifunctional chelating agent **4**, the synthesis and the characterization of the conjugated compounds **9**–**17**, the general procedure for the preparation of Gd complexes using GdCl₃, and the preparation of the ⁶⁸Ga-labeled compounds are reported in the Supporting Information.

Molecular modeling

All calculations were run using the Schrödinger suite of programs (<http://www.schrodinger.com>) through the Maestro graphical interface.

Protein setup

The crystal structure of the extracellular domain of the integrin $\alpha_v\beta_3$ receptor in complex with cilengitide (PDB ID: 1L5G)^[24b] was used for Monte Carlo conformational searches. Calculations were performed only on the globular head of the integrin because the

head group of integrin has been identified in the X-ray structure as the ligand binding region. The protein was truncated to residue sequences 41–342 for chain α and 114–347 for chain β . Due to a lack of parameters, the Mn²⁺ ions in the experimental protein structure were modeled by replacing them with Ca²⁺ ions. The resulting structure was prepared using the Protein Preparation Wizard of the graphical user interface Maestro. All nonpolar hydrogen atoms of the protein were removed except for the hydrogen atoms of aromatic residues within 3 Å of the X-ray structure ligand. The coordination shell of metal cation belonging to MIDAS (metal-ion-dependent adhesion site) and ADMIDAS (adjacent to MIDAS) was completed on the basis of the integrin $\alpha_{IIB}\beta_3$ X-ray structures^[26] by adding one and two water molecules, respectively.

Ligand setup

The X-ray structure of the Gd cage coordinated to one water molecule^[27] was linked to the bound-like conformation Inv γ (Asp)+ β [Gly,Asp] of the RGD cyclopeptide.^[11b] The distances of nitrogen and oxygen atoms coordinated to the Gd³⁺ ion were kept fixed by a force constant of 500 kJ mol⁻¹ Å².

Monte Carlo conformational searches

Monte Carlo conformational searches of compounds **9**(Gd) and **10**(Gd) (MCMM,^[28] AMBER* force field,^[22] implicit water GB/SA solvation model^[23]) were performed as implemented in the framework of MacroModel^[21] version 9.6 within the integrin $\alpha_v\beta_3$ binding site prepared as described in the protein setup. For each search, at least 1000 starting structures for each variable torsion angle were generated and minimized until the gradient was < 0.05 kJ Åmol⁻¹ using the truncated Newton–Raphson algorithm.^[29] Duplicate conformations of ligands and those with an energy > 6 kcal mol⁻¹ above the global minimum were discarded. Default parameters for ligand rotation and translation were used.

The substructure utility was used to model the receptor atoms. Residue atoms within 5 Å of X-ray ligand were constrained to crystallographic coordinates by a harmonic potential (with a force constant $K=100$ kJ mol⁻¹ Å² for atoms up to 3 Å and with $K=300$ kJ mol⁻¹ Å² for atoms between 3 and 5 Å) allowing the polar and aromatic hydrogen atoms free movement. Residue atoms between 5 and 10 Å were frozen to their X-ray position ($K=-1$). The remaining receptor atoms were ignored during the calculations.

Receptor binding assays

A 96-well microtiter plate was coated overnight at 4 °C with $\alpha_v\beta_3$ integrin (Chemicon; 0.5 μ g mL⁻¹, 100 μ L well⁻¹) in coating buffer (20 mM Tris-HCl pH 7.4, 150 mM NaCl, 1 mM MnCl₂, 0.5 mM MgCl₂, 2 mM CaCl₂). The plate was washed once with blocking buffer (1% BSA in coating buffer, 200 μ L well⁻¹) and then incubated in the same buffer (200 μ L well⁻¹) for 2 h at room temperature. Afterward, the plate was rinsed twice with blocking buffer and incubated (100 μ L well⁻¹, 3 h at room temperature) with various concentrations of test compounds (0.01–10 000 nM) in the presence of biotinylated vitronectin (1 μ g mL⁻¹). The plate was then washed three times with blocking buffer and incubated with streptavidin–HRP (Strep–HRP, GE Healthcare; 1:10 000 in PBS, 100 μ L well⁻¹) for 1 h at room temperature. After additional four washes in PBS, the plate was incubated with TMB solution (Sigma–Aldrich; 100 μ L well⁻¹) for 3–5 min, and the colorimetric reaction was stopped by adding 50 μ L 2 N H₂SO₄. To quantify competitive binding, we determined the remaining bound biotinylated vitronectin by reading the ab-

sorbance values at λ 450 nm. All assays were carried out in triplicate and repeated 2–3 times. IC₅₀ values were determined by non-linear regression analysis using GOSA-fit software (Global Optimisation by Simulated Annealing; <http://www.bio-log-software.com/>).

Relaxometry

Experimental details describing the measurement of gadolinium concentration and millimolar relaxivity at 20 MHz are reported in the Supporting Information. NMRD profiles of compounds **9**(Gd)–**12**(Gd) at 25 °C, $r_{1\rho}$ dependence from temperature, and correlation between relaxivity and molecular weight for $\alpha_v\beta_3$ integrin targeting contrast agents are also given in the Supporting Information (figures S3–S5).

Animal models

Human glioblastoma cells (U-87 MG) were supplied by the ATCC. Cells were grown in EMEM supplemented with 10% fetal bovine serum, 2 mM glutamine, 100 IU mL⁻¹ penicillin, and 100 μ g mL⁻¹ streptomycin. CD-1 nude mice (six-week-old females) were supplied by Charles River. All procedures involving animals were conducted according to national and international laws on animal experimentation (L.D. 116/92; C.D. EEC 86/609). No validated non-animal alternatives were known to meet the objectives of this study. U-87 MG cells (5×10^6) were resuspended in 0.1 mL PBS and injected subcutaneously in the right flank of each mouse. Four weeks after cell inoculation, animals were used for PET experiments.

PET experiments

The aim of this study was to evaluate the uptake of **15**(⁶⁸Ga) administered in a xenograft mouse model of human glioblastoma (U-87 MG) cells in CD1 nude mice. U-87 MG cells were collected and washed two times with PBS; cells (5×10^6) were resuspended in 0.1 mL PBS and injected subcutaneously in the right flank of each six-week-old female mouse. Four weeks after, animals were anaesthetized with isoflurane gas (1% in oxygen). During the experiments, anaesthesia was maintained by adjustment of the gas level as a function of breathing rate. All the animals were warmed with a heating pad (30 °C) for 30 min before injection up to the end of the PET experiment. **15**(⁶⁸Ga) or ⁶⁸Ga(AAZTA) were administered intravenously at the mean dose of 250 μ Ci per mouse. In one experiment, c(RGDfV) (10 mg kg⁻¹) was administered simultaneously with **15**(⁶⁸Ga). PET experiments were performed on a YAP-(S)PET scanner (I.S.E. Ingegneria dei Sistemi Elettronici s.r.l., Pisa, Italy). Uptake in tumor tissue was determined at various time points up to 150 min and is expressed as the standardized uptake value (SUV).

Acknowledgements

We gratefully acknowledge the Ministero dell'Università e della Ricerca, MIUR (PRIN prot. 2008J4YNJY, FIRB RBNE03LF7X) for financial support. Expert assistance in relaxivity measurements by Luisa Poggi (Bracco Imaging SpA, Bracco Research Centre, Via Ribes 5, 10010 Colletterto Giacosa (TO) Italy) is also gratefully acknowledged.

Keywords: chelates · imaging agents · integrins · RGD · tumor targeting

- [1] D. A. Torigian, S. S. Huang, M. Houseni, A. Alavi, *CA-Cancer J. Clin.* **2007**, *57*, 206–224.
- [2] T. E. Peterson, H. C. Manning, *J. Nucl. Med. Technol.* **2009**, *37*, 151–161.
- [3] R. van der Meel, W. M. Gallagher, S. Oliveira, A. E. O'Connor, R. M. Schiffelers, A. T. Byrne, *Drug Discovery Today* **2010**, *15*, 102–114.
- [4] a) E. Ruoslahti, *Annu. Rev. Cell Dev. Biol.* **1996**, *12*, 697–715; b) X. Lu, D. Lu, M. F. Sculli, V. V. Kakkar, *Curr. Pharm. Des.* **2008**, *14*, 2140–2158.
- [5] a) J. D. Hood, D. A. Cheresh, *Nat. Rev. Cancer* **2002**, *2*, 91–100; b) J. S. Desrosellier, D. A. Cheresh, *Nat. Rev. Cancer* **2010**, *10*, 9–22; c) C. Ruegg, A. Mariotti, *Cell. Mol. Life Sci.* **2003**, *60*, 1135–1157.
- [6] a) S. M. Albelda, S. A. Mette, L. Damjanovich, D. E. Elder, R. M. Stewart, M. Herlyn, C. A. Buck, *Cancer Res.* **1990**, *50*, 6757–6764; b) N. P. McCabe, S. De, A. Vasani, J. Brainard, T. V. Byzova, *Oncogene* **2007**, *26*, 6238–6243; c) L. Bello, M. Francolini, P. Marthyn, J. Zhang, R. S. Carroll, D. C. Nikas, J. F. Strasser, R. Villani, D. A. Cheresh, P. M. Black, *Neurosurgery* **2001**, *49*, 380–389.
- [7] a) G. Gasparini, P. C. Brooks, E. Biganzoli, P. B. Vermeulen, E. Bonoldi, L. Y. Dirix, G. Ranieri, D. A. Cheresh, *Clin. Cancer Res.* **1998**, *4*, 2625–2634; b) A. Vonlaufen, G. Wiedle, B. Borisch, S. Birrer, P. Lauder, B. A. Imhof, *Mod. Pathol.* **2001**, *14*, 1126–1132.
- [8] a) M. A. Horton, *Int. J. Biochem. Cell. Biol.* **1997**, *29*, 721–725; b) M. A. Arnaout, S. L. Goodman, J. P. Xiong, *Curr. Opin. Cell Biol.* **2002**, *14*, 641–651.
- [9] a) R. Haubner, R. Gratias, B. Diefenbach, S. L. Goodman, A. Jonczyk, H. Kessler, *J. Am. Chem. Soc.* **1996**, *118*, 7461–7472; b) J. W. Smith, *Curr. Opin. Investig. Drugs* **2003**, *4*, 741–745; c) M. A. Dechantsreiter, E. Plankner, B. Mathä, E. Lohof, G. Hölzemann, A. Jonczyk, S. L. Goodman, H. Kessler, *J. Med. Chem.* **1999**, *42*, 3033–3040.
- [10] a) L. Belvisi, A. Bernardi, A. Checchia, L. Manzoni, D. Potenza, C. Scolastico, M. Castorina, A. Cupelli, G. Giannini, P. Carminati, C. Pisano, *Org. Lett.* **2001**, *3*, 1001–1004; b) L. Belvisi, T. Riccioni, M. Marcellini, I. Chiarucci, D. Efrati, L. Vesci, D. Potenza, C. Scolastico, L. Manzoni, K. Lombardo, M. A. Stasi, B. Nico, D. Ribatti, M. Presta, P. Carminati, C. Pisano, *Mol. Cancer Ther.* **2005**, *4*, 1670–1680; c) D. Arosio, L. Belvisi, L. Colombo, M. Colombo, D. Invernizzi, L. Manzoni, D. Potenza, M. Serra, M. Castorina, C. Pisano, C. Scolastico, *ChemMedChem* **2008**, *3*, 1589–1603.
- [11] L. Manzoni, D. Arosio, L. Belvisi, A. Bracci, M. Colombo, D. Invernizzi, C. Scolastico, *J. Org. Chem.* **2005**, *70*, 4124–4132; b) L. Manzoni, L. Belvisi, D. Arosio, M. Civera, M. Pilkington-Miksa, D. Potenza, A. Caprini, E. M. V. Araldi, E. Monferini, M. Mancino, F. Podestà, C. Scolastico, *ChemMedChem* **2009**, *4*, 615–632.
- [12] a) D. Arosio, L. Manzoni, M. E. Araldi, A. Caprini, E. Monferini, C. Scolastico, *Bioconjugate Chem.* **2009**, *20*, 1611–1617; b) S. Lanzardo, L. Conti, C. Brioschi, M. P. Bartolomeo, D. Arosio, L. Belvisi, L. Manzoni, A. Maiocchi, F. Maisano, G. Forni, *Contrast Media Mol. Imaging* **2011**, *6*, 449–458.
- [13] a) C. F. G. C. Geraldès, S. Laurent, *Contrast Media Mol. Imaging* **2009**, *4*, 1–23; b) A. E. Merbach, E. Tóth, *The Chemistry of Contrast Agents in Medical Magnetic Resonance*, Wiley, New York, **2001**.
- [14] P. Caravan, J. J. Ellison, T. J. McMurphy, R. B. Lauffer, *Chem. Rev.* **1999**, *99*, 2293–2352.
- [15] D. E. Reichert, J. S. Lewis, C. J. Anderson, *Coord. Chem. Rev.* **1999**, *184*, 3–66.
- [16] S. Aime, L. Calabi, C. Cavallotti, E. Gianolio, G. B. Giovenzana, P. Losi, A. Maiocchi, G. Palmisano, M. Sisti, *Inorg. Chem.* **2004**, *43*, 7588–7590.
- [17] a) L. Lattuada, A. Barge, G. Cravotto, G. B. Giovenzana, L. Tei, *Chem. Soc. Rev.* **2011**, *40*, 3019–3049; b) L. M. De León-Rodríguez, Z. Kovacs, *Bioconjugate Chem.* **2008**, *19*, 391–402; c) J. Fichna, A. Janecka, *Bioconjugate Chem.* **2003**, *14*, 3–17; d) M. Woods, Z. Kovacs, A. D. Sherry, *J. Supramol. Chem.* **2002**, *2*, 1–15.
- [18] P. L. Anelli, F. Fedeli, O. Gazzotti, L. Lattuada, G. Lux, F. Rebasti, *Bioconjugate Chem.* **1999**, *10*, 137–140.
- [19] A. Heppeler, S. Froidevaux, H. R. Mäcke, E. Jermann, M. Béhé, P. Powell, M. Hennig, *Chem. Eur. J.* **1999**, *5*, 1974–1981.
- [20] A. Barge, E. Cappelletti, G. Cravotto, A. Ferrigato, L. Lattuada, F. Marinoni, L. Tei, *Org. Biomol. Chem.* **2009**, *7*, 3810–3816.
- [21] MacroModel version 9.6, Schrödinger LLC, New York, NY (USA), **2008**.

- [22] S. J. Weiner, P. A. Kollman, D. T. Nguyen, D. A. Case, *J. Comput. Chem.* **1986**, *7*, 230–252.
- [23] W. C. Still, A. Tempczyk, R. C. Hawley, T. Hendrickson, *J. Am. Chem. Soc.* **1990**, *112*, 6127–6129.
- [24] a) J.-P. Xiong, T. Stehle, B. Diefenbach, R. Zhang, R. Dunker, D. L. Scott, A. Joachimiak, S. L. Goodman, M. A. Arnaout, *Science* **2001**, *294*, 339–345; b) J.-P. Xiong, T. Stehle, R. Zhang, A. Joachimiak, M. Frech, S. L. Goodman, M. A. Arnaout, *Science* **2002**, *296*, 151–155.
- [25] S. Aime, A. Barge, C. Cabella, S. G. Crich, E. Gianolio, *Curr. Pharm. Biotechnol.* **2004**, *5*, 509–518.
- [26] T. A. Springer, J. Zhu, T. Xiao, *J. Cell Biol.* **2008**, *182*, 791–800.
- [27] M. B. Inoue, M. Inoue, Q. Fernando, *Inorg. Chim. Acta* **1995**, *232*, 203–206.
- [28] G. Chang, W. C. Guida, W. C. Still, *J. Am. Chem. Soc.* **1989**, *111*, 4379–4386.
- [29] J. W. Ponder, F. M. Richards, *J. Comput. Chem.* **1987**, *8*, 1016–1024.

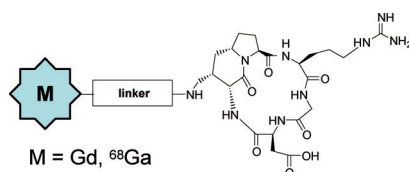
Received: January 21, 2012

Revised: March 12, 2012

Published online on ■ ■ ■ ■, 0000

FULL PAPERS

Persistence pays: Novel Gd and ^{68}Ga chelates conjugated with a cyclic RGD peptidomimetic integrin ligand were prepared. Preliminary in vivo evaluation of the first integrin-targeted AAZTA- (^{68}Ga) complex showed good uptake and persistence in a xenograft mouse model of human glioblastoma (U-87 MG) cells.



L. Manzoni,* L. Belvisi,* D. Arosio,
M. P. Bartolomeo, A. Bianchi, C. Brioschi,
F. Buonsanti, C. Cabella, C. Casagrande,
M. Civera, M. De Matteo, L. Fugazza,
L. Lattuada, F. Maisano, L. Miragoli,
C. Neira, M. Pilkington-Miksa,
C. Scolastico



**Synthesis of Gd and ^{68}Ga Complexes
in Conjugation with
a Conformationally Optimized RGD
Sequence as Potential MRI and PET
Tumor-Imaging Probes**

